NANO LETTERS

Letter

pubs.acs.org/NanoLett

Large Electroabsorption Susceptibility Mediated by Internal Photoconductive Gain in Ge Nanowires

Hyun-Seung Lee,[†] Cheol-Joo Kim,[‡] Donghun Lee,[†] Ru Ri Lee,[‡] Kibum Kang,[†] Inchan Hwang,[‡] and Moon-Ho Jo*,[†]

[†]Department of Materials Science and Engineering, Yonsei University, Seongsan-No 262 Seodaemun-Gu, Seoul 120-749, Korea

[‡]Department of Materials Science and Engineering, Pohang University of Science and Technology, San 31, Hyoja-Dong, Nam Gu, Pohang, Gyungbuk 790-784, Korea

Supporting Information

ABSTRACT: Large spectral modulation in the photon-to-electron conversion near the absorption band-edge of a semiconductor by an applied electrical field can be a basis for efficient electro-optical modulators. This electro-absorption effect in Group IV semiconductors is, however, inherently weak, and this poses the technological challenges for their electro-photonic integration. Here we report unprecedentedly large electro-absorption susceptibility at the direct band-edge of intrinsic Ge nanowire (NW) photodetectors, which is strongly diameter-dependent. We provide evidence that the large spectral shift at the 1.55 μm wavelength, enhanced up to 20 times larger than Ge bulk crystals, is attributed to the internal Franz–Keldysh effect across the NW surface field of ~10^5 V/cm, mediated by the strong photoconductive gain. This classical size-effect operating at the nanometer scale is universal, regardless of the choice of materials, and thus suggests general implications for the monolithic integration of Group IV photonic circuits.

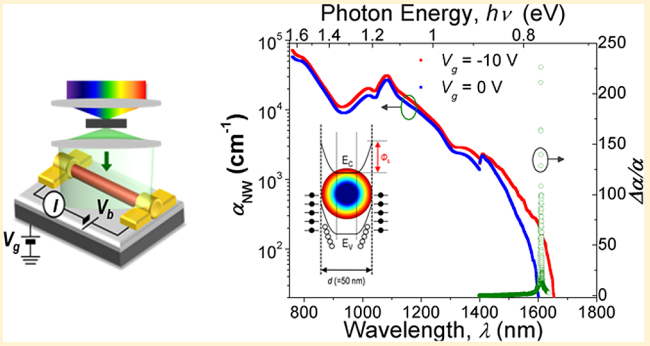

KEYWORDS: *Electro-optical modulation, photoconductive gain, photodetector, Group IV photonics, Ge nanowires, Franz–Keldysh effect*

Energy band distortion under a strong potential gradient (typically 10^5–10^6 V/cm) shifts the absorption edge of the direct band gap (E_g) to a lower energy by the Franz–Keldysh (F–K) effect.[1,2] Silicon crystals, however, require the very high fields close to the breakdown field to obtain a substantial F–K effect.[3,4] Germanium has been recognized as a promising candidate for photodetectors and electro-optical modulators,[5,6] as it displays the quantum-confined Stark effect in $Si_{1-x}Ge_x$ quantum wells and the direct-band transition characteristics in tensile-strained Ge thin films near the telecommunication wavelength.[7−13] Although low-dimensional semiconductors, such as colloidal quantum dots and nanowires (NWs) exhibit substantially large spectral changes and optical gain in light absorption, due to the dielectric, optical, and electronic confinements,[14−19] size-dependent electroabsorption processes in Ge nanocrystals have been scarcely addressed in a quantitative manner and yet to be fully exploited.[6,20,21] A strong photoconductive gain effect in Ge NWs, arising from the temporal charge separation at the NW surfaces, has been observed to significantly influence the photodetection characteristics near the direct band gap.[22−25] Therein, the high surface-state density in Ge NWs and the associated carrier separation often produce a strong electrostatic field in excess of 10^5 V/cm in the NW radial direction near the surfaces. In this work, we have systematically investigated diameter-dependent electroabsorption processes by tuning the internal field of Ge NWs with the gate (V_g) and bias voltage (V_b) and attributed our observations to the internal F–K effect, by which large spectral modulation is further amplified by the photoconductive gain during the interband photocarrier generation and transport.

The upper inset of Figure 1a shows the schematics of a Ge NW photodetector, where the intrinsic (nominally undoped) Ge NW of a given diameter (50–130 nm) is ohmic-contacted to Ni/Au electrodes (source and drain) (see also Supporting Information) and is also gated across a SiO_2 dielectric layer by a degenerate Si substrate (gate). We have verified that our Ge NWs commonly show the *p*-type photoconductor characteristics, consistent with literature, as in the lower inset. We have obtained the photocurrent (I_{ph}) spectra at the photon wavelength of 0.45–1.8 μm, when a white-light supercontinuum laser source coupled to a monochromator as a wavelength tunable excitation system illuminates over the area

Received: September 6, 2012
Revised: October 16, 2012
Published: October 25, 2012

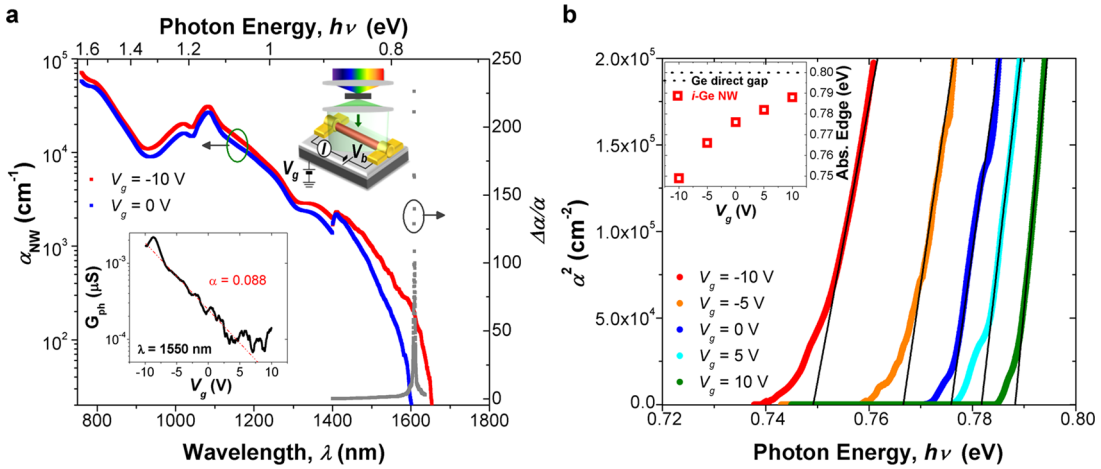

Figure 1. Gate-field dependent absorption spectra of Ge NW photodetectors (a) Optical absorption spectra obtained from the photocurrent data of a Ge NW photodetector. The dotted gray line with the right axis exhibits the spectral absorption contrast ratio, $\Delta\alpha/\alpha$, at the absorption edge. The upper inset illustrates the schematics of photodetection experiments of Ge NW field-effect transistor with the wavelength tunable excitation system. The whole active region of the devices was globally illuminated. The lower inset shows the *p*-type characteristics of photoconductance at λ = 1550 nm with the gate efficiency, α of 0.088. (b) The gate voltage dependent absorption spectra near the direct band gap of Ge NWs. Apparent absorption onset values were extracted from the squared absorption coefficient spectra for different gate voltages by extrapolating the linear portions. The inset is the absorption edge values as a function of gate voltages which shows a large span of the shift over the 50 meV.

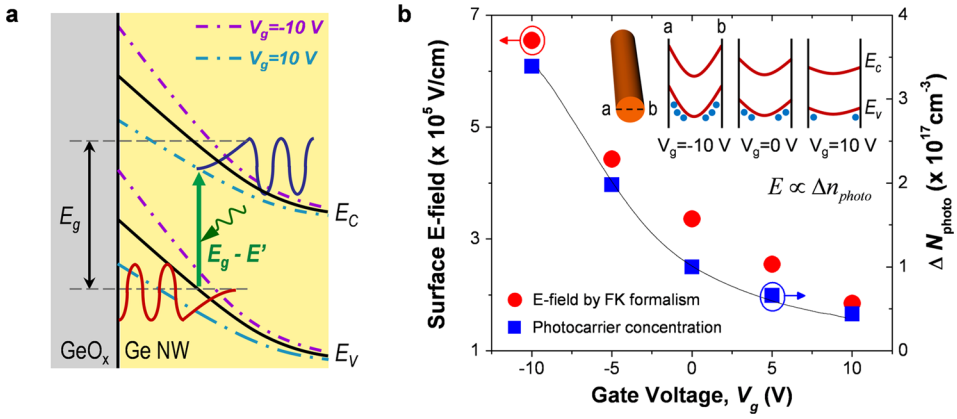

Figure 2. Electro-absorption modulation by F−K effect in Ge NW photodetectors (a) Illustration of the energy band bending near the Ge NW surface indicating the internal F−K effect. An effective wave function overlap between electrons in the conduction band and holes in the valence band penetrates the classical E_g under the presence of the effectively large electrical field, ensuing the sub-E_g optical transition. (b) Gate voltage dependence of surface electric field estimated by F−K formalism (left axis) and experimentally obtained photocarrier concentration (right axis). The inset illustrates the band bending inside the NW for different gate voltages of −10 V, 0 V, and 10 V.

containing the NW photodetector, as seen in the main panel of Figure 1a. The directly measured I_{ph} is converted into the effective absorption coefficient, α, by the relation[26] of

$$\alpha = -\frac{1}{d}\ln\left(1 - \frac{I_{ph}}{(1-R)}\cdot\frac{h\nu}{G\cdot e\cdot\eta\cdot P}\right) \quad (1)$$

where d is the diameter of the Ge NW, R is the reflectance, G is the photoconductive gain, η is the photon-to-carrier conversion efficiency, and P is the incident optical power (also see Supporting Information). We assume that η is equal to unity, and the change in the surface reflection upon the applied field is negligible.[11,13] Notably, the spectral on-set of the measurable I_{ph} near the 1.5−1.6 μm wavelength, which corresponds to the direct band gap edge of Ge, shifts significantly to a lower energy upon decreasing V_g from 0 V to −10 V, although the spectral features above the band gap energy remains constant. We have also plotted the spectral absorption contrast ratio, $\Delta\alpha/\alpha$, to express the efficiency of modulation of light absorption, showing a narrow peak variation at the absorption edge. This variation is at least one or 2 orders of magnitude larger than in literature.[6,11,12,27] Figure 1b is the photoresponsivity by the relation of $I_{ph} \sim \exp(\alpha) \sim \exp(h\nu - E_g)^{1/2}$ for the direct gap transition near the absorption edge in a 80 nm thick Ge NW as a function V_g in the ±10 V range, showing the large span of the absorption edge shift of 50 meV. Conventionally, Si optical modulators exploit the plasma dispersion effect, where the variation in the free carrier concentration changes the effective absorption coefficient.[1,28] We assessed the changes in absorption coefficient due to the free carrier effect based on an analytical dispersion relation between the carrier concentration and the absorption coefficient derived from the Drude−Lorenz equation by Soref et al.[28] and found that the observed $\Delta\alpha$ is higher by at least 2 orders of magnitude. Thus, we exclude the free carrier absorption effect for the principal origin of our observations. Instead, we attempt to analyze our observations within the framework of the F−K effect, by which

dx.doi.org/10.1021/nl3033203 | Nano Lett. 2012, 12, 5913−5918

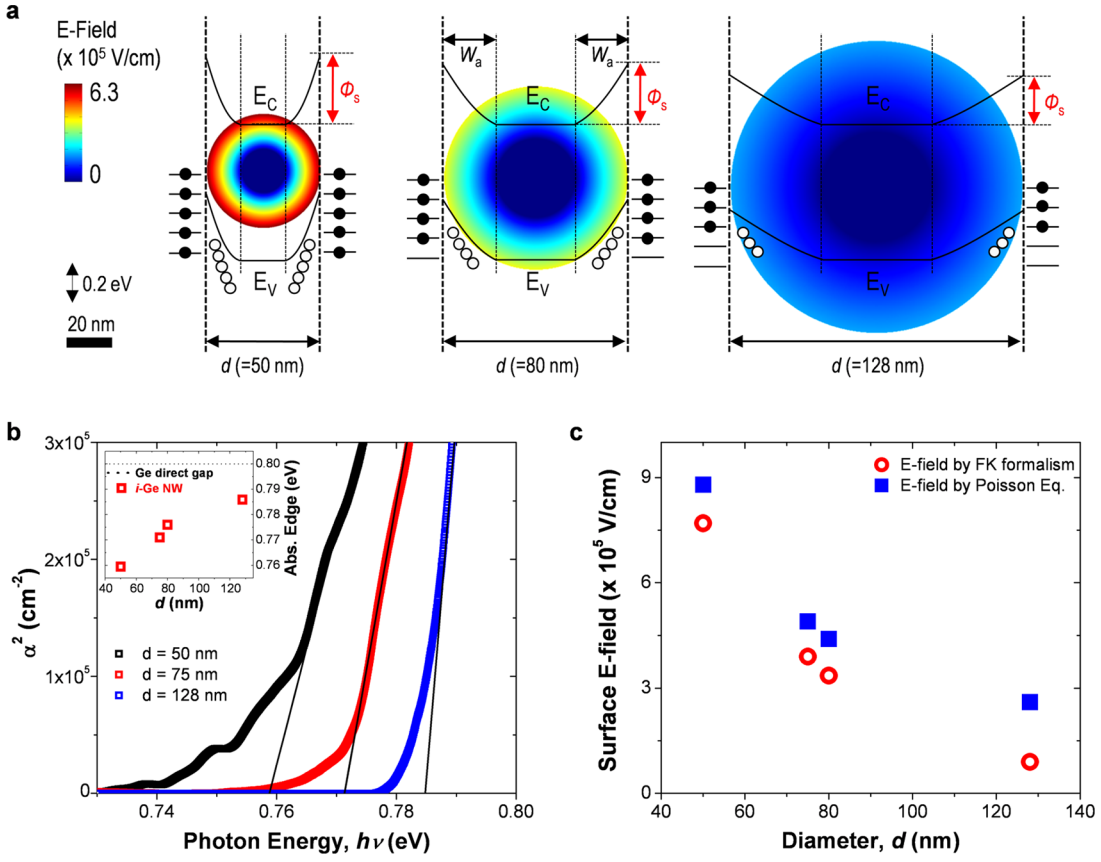

Figure 3. Diameter-dependent electro-absorption modulation in Ge NW photodetectors. (a) Two-dimensional electrostatic field distribution plots for different diameter values plotted in color scale by solving the Poisson equation with the COMSOL multiphysic software. The band diagrams for the cross-section of Ge NWs with the diameters of 50, 80, and 128 nm are described by black lines and overlaid with the simulated two-dimensional electrostatic field distribution in colors. The relative position of states and the numbers of black (trapped electrons) and white (accumulated holes) circles are only conceptually represented for the effective numbers of carriers and the surface potentials. (b) The squared absorption coefficient spectra for different diameters, from which the apparent absorption onset values can be extracted by extrapolating the linear portions. Inset: Absorption edge values as a function of NW diameters. (c) Comparison of the diameter dependence of surface electric field between the electric field experimentally obtained by F−K formalism and the electric field calculated by the Poisson equation.

the sub-E_g optical transition can be available via an effective wave function overlap that penetrates the classical E_g under the presence of the effectively large electrical field, as seen in Figure 2a. Therein the electron wave function modifies into Airy function, and the relevant α decays exponentially below the E_g as expressed by[29]

$$\alpha \sim \exp\left[-\left|\frac{h\nu - E_g}{E'}\right|^{3/2}\right] \quad (2)$$

$$E' = \frac{2(e\cdot\hbar\cdot E_{field})^{2/3}}{3(m_r^*)^{1/3}} \quad (3)$$

where m_r^* is the reduced effective mass and the absorption edge shifts to the lower energy with increasing the applied electric field. From eq 3, the observed absorption edge shift of 50 meV requires the static field on the order of $\sim 10^5$ V/cm, applied across the Ge direct E_g. We attribute the physical origin of this internal surface field to the temporal separation of photogenerated carriers near the NW surfaces, as in the inset of Figure 2b. Ge surface states located in the GeO_x and the interface between Ge and GeO_x tend to preferentially trap the photogenerated electrons, leaving the free holes in the NW inner body,[23,30−32] and this spatial charge separation generates an effectively large surface field in the NW radial direction, $E(r)$, which can be estimated by solving Poisson equation in a cylindrical geometry as,

$$E(r) = \frac{eN}{2\varepsilon}\left(r - \frac{(d/2 - W_d)^2}{r}\right) \quad \text{and} \quad W_d = \sqrt{\frac{4\varepsilon\phi_s}{eN}} \quad (4)$$

where N, r, d, ε, and ϕ_s are the effective accumulated photocarrier concentration, the cylinder radius, the NW diameter, electrical permittivity, and the surface potential. Here we assume that the depletion layer width (W_d) is smaller than r in the cylindrical model. Then, this internal electrostatic field is principally dependent on the photoinduced charge density, N, which can be tuned by the applied V_g. We deduced the photoinduced hole carrier density from the I_{ph}-trans-conductance measurement and plotted them in Figure 2b along with the field strength required to observe the magnitude by the internal F−K effect in eq 2. The comparison shows that the carrier density variation on the order of $\sim 10^{17}$ cm^{-3} is closely related to a variation of the internal field in the 10^5 V/cm range. This agreement suggests that the variation in the strong surface field, modulated by the photoinduced carrier density with the applied V_g, is responsible for the observed absorption edge shift.

dx.doi.org/10.1021/nl3033203 | Nano Lett. 2012, 12, 5913−5918

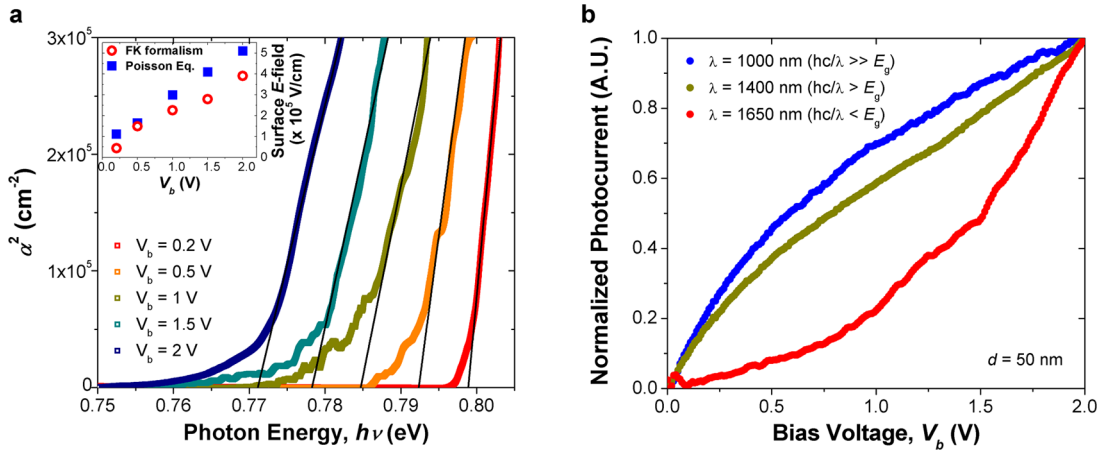

Figure 4. Bias-voltage dependent electroabsorption in Ge NW photodetectors. (a) Bias-voltage dependence of the absorption spectra near the direct band gap of Ge for different bias voltages of 0.2, 0.5, 1, 1.5, and 2 V. From the squared absorption spectra for different bias-voltages, the apparent absorption onset values were extracted by extrapolating the linear portions. Inset: Comparison of the bias voltage dependence between the surface electric field experimentally obtained by F−K formalism and the field calculated by the Poisson equation. (b) Comparison of the normalized photocurrent as a function of bias voltage at the incident light of different wavelengths in the Ge NW device with the diameter of 50 nm.

In our simple cylindrical capacitor model of a Ge NW with the capacitance C and the effective cross-sectional area of A, the number of the electron−hole pairs created at a NW cross-section per unit length (l) is proportional to $A\,l \sim \pi(d/2)^2 l$, and the number of surface trapped electrons per unit length is proportional to $2\pi(d/2)\,l$. Provided that the number of the photoinduced charges is directly proportional to the number of surface-trapped electrons by an electrostatic interaction, the accumulated hole concentration, N can be expressed by $N \propto (Q/A) \propto [(2\pi\cdot(d/2))/(\pi\cdot(d/2)^2)] \propto (1/d)$.[24] Then, one can expect that the smaller d lifts the surface potential significantly due to the higher surface charge density. Two-dimensional electrostatic field distribution plots for different d values are plotted in Figure 3a by solving eq 4 under the constant photon injection rate. We have measured the I_{ph}-spectral changes near the absorption edge as a function of d at V_b = 2 V and V_g = 0 V, and the converted α is plotted in Figure 3b. Indeed, the larger edge shift, with decreasing d from 128 to 50 nm, was clearly observed. The comparison between the calculated surface E-field by eq 4 with the E-field strength required for the observed diameter-dependent F−K effects by the eq 3 find a reasonable agreement, as in Figure 3c. This observation strongly corroborates that the internal F−K effect is responsible for the observed large electro-optical effects.

The fact that the large internal field at the NW surface is modulated by the degree of the surface-state filling of the photogenerated carriers raises an intriguing possibility that the electroabsorption can be amplified by the photoconductive gain upon the interband optical transition across the E_g. The photoconductive gain is defined as the ratio between the photocarrier lifetime (τ) and their transit time in the photoconductor channel during the photodetection process; thus in the NW photoconductors it is strongly influenced by the temporal and spatial carrier separation near the NW surface.[22,23] For example, the photocarrier recombination in Ge NWs is delayed by the electron trapping at the surface/interface-states, ensuing the prolonged lifetime, and as a result the photoconductive gain is achieved. Then, the bias-voltage (V_b), applied across the ohmic NW channel, can control the electroabsorption effects by the carrier concentration modulation, associated with the degree of the surface-state filling, as suggested in the following. Figure 4 is the I_{ph}-spectra as a function of V_b at the low voltage range from 0.2 to 2 V in a 75 nm thick Ge NW and clearly shows that the absorption edge shifts significantly to a lower energy with increasing V_b near the direct E_g. The I_{ph} in the ohmic NW photoconductor of the cross-sectional area A is defined as,

$$I_{ph} = \frac{V_b}{L}(\mu_n + \mu_p)NeA \tag{5}$$

where L is the NW channel length, $\mu_{p(n)}$ is the photogenerated hole (electron) mobility, and N is the induced photocarrier concentration. At a steady-state photocarrier generation-recombination process, N is linearly proportional to its lifetime, τ, in a relation of

$$N = \frac{\eta(P_{opt}/h\nu)}{A\cdot L}\cdot\tau \tag{6}$$

where η is the photon-to-photocarrier conversion efficiency, and P_{opt} is the absorbed optical power. Interestingly, in our Ge NWs, we find that the τ is nonlinear to the V_b and strongly dependent on the photon wavelength (λ). The normalized I_{ph}−V_b at the different λ, in Figure 4b, clearly marks the transition from superlinear below the E_g to sublinear above the E_g. Provided that $\mu_{h(e)}$ is independent of V_b, the slope of $\Delta I_{ph}/\Delta V_b$ is connected to the ΔN in eq 5, which is in turn proportional to the $\Delta\tau$. This nonlinear I_{ph}−V_b characteristics at the different λ can be attributed to the degree of the surface-state filling of the photogenerated carriers during the photocarrier detection; while at $hc/\lambda > E_g$ the available surface-states are immediately filled and $\partial N/\partial V_b \sim \partial\tau/\partial V_b < 0$ within the applied V_b range, at $hc/\lambda \sim E_g$ the available surface-states are steadily filling with increasing V_b and $\partial N/\partial V_b \sim \partial\tau/\partial V_b > 0$. Thus, the increasing V_b near the E_g can progressively establish the significant ΔN, ensuing the efficient surface-field to enhance the F−K effect. This is also consistent with the power-dependent internal gain measurement in the Supporting Information. For a check-up, we deduced the surface field from the photocarrier concentration by eq 4 and found an excellent agreement with the field gradient required for the V_b-dependent F−K effects, as in the inset of Figure 4a.

dx.doi.org/10.1021/nl3033203 | Nano Lett. 2012, 12, 5913−5918

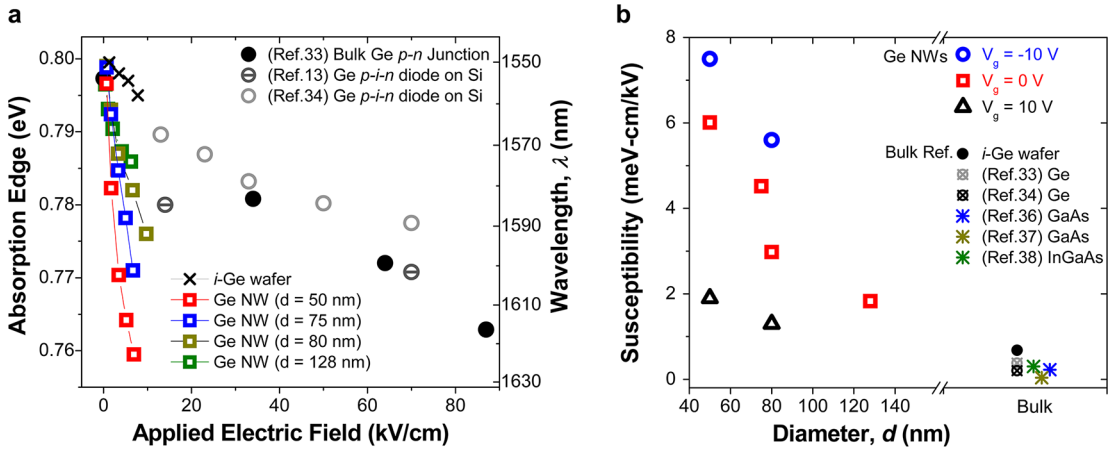

Figure 5. Large electro-absorption susceptibility in Ge NW photodetectors. (a) Summarized absorption edge shifts from various Ge NW diameters in our study as a function of the applied electric field, in comparison with those previously reported in bulk Ge photodetectors. (b) Electro-absorptive susceptibilities as a function of diameters for the gate voltage of −10, 0, and 10 V. Electro-absorption susceptibilities, previously reported for bulk Ge, GaAs, and InGaAs are also plotted for comparison.

The degree of the absorption edge shift in response to the applied field is quantitatively defined as electroabsorption susceptibility and represents a direct measure of the electro-optical modulation. Figure 5a summarizes such absorption edge shifts from various NW diameters in our study as a function of the applied field, in comparison with those previously reported in bulk Ge photodetectors. Clearly it shows a strong diameter dependence, where the thinnest Ge NW (50 nm) requires the substantially smaller field below 10 kV/cm of the externally applied field to generate the 40 meV shift. Equivalently, in Figure 5b, the measured electroabsorption susceptibility in our Ge NWs at their direct band-gaps is summarized, and it is recorded up to 7.5 meV·cm/kV at the 1.55 μm wavelength for the thinnest NW (50 nm), and this corresponds to the variation of the large absorption ($\Delta\alpha$) of 1345 cm^{-1}. It is as large as the 20 times of the best known Ge electro-optical modulator, fabricated from the various forms of bulk Ge crystals including thin films[33] and $p-i-n$ photodiodes.[11,34] In fact, it is even much higher than those ever reported from direct-gap semiconductors such as InP[35] and InGaAs.[36−38]

Methods. *Ge NWs Synthesis and Photodetector Fabrication.* Single-crystalline Ge NWs in our study were synthesized by Au catalyst-assisted chemical vapor syntheses. We prepared Au catalysts on SiO_2/Si substrate by dispersion of 20−50 nm colloidal Au nanoparticles or evaporation of 0.5−2 nm Au thin film. Then the samples were loaded in a hot wall CVD chamber, and the temperature of furnace was heated to 330 °C; H_2 was injected until the total pressure reached to 200 Torr. Subsequently 10% of GeH_4 premixed in H_2 precursors and H_2 gas were injected into the furnace with each flow rate of 150 sccm. A two-step GeH_4 CVD process was performed by controlling the temperature from 330 to 270 °C to suppress the side-wall growth. Then, Ge NW devices were fabricated on 100 nm SiO_2/p-type degenerated Si substrates by standard e-beam lithography and the Ni/Au (30/150 nm) metallization by thermal evaporation. The degenerated silicon substrate was used as a global backgate.

Spectral Photocurrent Measurements. For the spectral photocurrent measurements, we used a broadband supercontinuum laser (450 nm $\leq \lambda \leq$ 2000 nm) combined with a monochromator for the high resolution spectra. During the wavelength scanning, photocurrent is measured by a lock-in technique with the chopper frequency of 10 kHz and subsequently normalized to the photon flux. The chopped laser beam is focused by microscopic lens (NA = 0.5) and illuminates the NW channel region of devices.

■ ASSOCIATED CONTENT

Supporting Information

Light absorption and photodetection characteristics of Ge nanowires. This material is available free of charge via the Internet at http://pubs.acs.org.

■ AUTHOR INFORMATION

Corresponding Author

*E-mail: mhjo@yonsei.ac.kr.

Notes

The authors declare no competing financial interest.

■ ACKNOWLEDGMENTS

This work was supported by Basic Science Research Program (2010-0017853), MEST-AFOSR NBIT Phase II (K20716000006-07A0400-00610), Nano Original & Fundamental Technology R&D Program (20120006217), ERC Program (2010-0001873), and Global Frontier Research Program (2011-0031639) through the NRF funded by the MEST.

■ REFERENCES

(1) Franz, W. *Z. Naturforsch.* **1958**, *13a*, 484−489.
(2) Keldysh, L. V. *Sov. Phys. J. Exp. Theor. Phys.* **1958**, *34*, 788−790.
(3) Reed, G. T.; Mashanovich, G.; Gardes, F. Y.; Thomson, D. J. *Nat. Photon.* **2010**, *4*, 518−526.
(4) Leuthold, J.; Koos, C.; Freude, W. *Nat. Photon.* **2010**, *4*, 535−544.
(5) Lauhon, L. J.; Gudiksen, M. S.; Wang, D.; Lieber, C. M. *Nature* **2002**, *420*, 57−61.
(6) Greytak, A. B.; Barrelet, C. J.; Li, Y.; Lieber, C. M. *Appl. Phys. Lett.* **2005**, *87*, 151103.
(7) Frova, A.; Handler, P.; Germano, F. A.; Aspnes, D. E. *Phys. Rev.* **1966**, *145*, 575−583.
(8) Kuo, Y. H.; Lee, Y. K.; Ge, Y.; Ren, S.; Roth, J. E.; Kamins, T. I.; Miller, D. A. B.; Harris, J. S. *Nature* **2005**, *437*, 1334−1336.
(9) Assefa, S.; Xia, F.; Vlasov, Y. A. *Nature* **2010**, *464*, 80−84.

(10) Tang, L.; Kocabas, S. E.; Latif, S.; Okyay, A. K.; Gagnon, D. D.; Saraswat, K. C.; Miller, D. A. B. *Nat. Photon.* **2008**, *2*, 226−229.
(11) Michel, J.; Liu, J.; Kimerling, L. C. *Nat. Photon.* **2010**, *4*, 527−534.
(12) Liu, J.; Beals, M.; Pomerene, A.; Bernardis, S.; Sun, R.; Cheng, J.; Kimerling, L. C.; Michel, J. *Nat. Photon.* **2008**, *2*, 433−437.
(13) Jongthammanurak, S.; Liu, J.; Wada, K.; Cannon, D. D.; Danielson, D. T.; Pan, D.; Kimerling, L. C.; Michel, J. *Appl. Phys. Lett.* **2006**, *89*, 161115.
(14) Klimov, V. I.; Mikhailovsky, A. A.; Xu, S.; Malko, A.; Hollingsworth, J. A.; Leatherdale, C. A.; Eisler, H. J.; Baewndi, M. G. *Science* **2000**, *290*, 314−317.
(15) Cao, L.; White, J. S.; Park, J. S.; Schuller, J. A.; Clemens, B. M.; Brongersma, M. L. *Nat. Mater.* **2009**, *8*, 643−647.
(16) Konstantatos, G.; Sargent, E. H. *Nat. Nanotechnol.* **2010**, *5*, 391−400.
(17) Schaller, R. D.; Klimov, V. I. *Phys. Rev. Lett.* **2004**, *92*, 186601.
(18) Konstantatos, G.; Howard, I.; Fischer, A.; Fischer, A.; Hoogland, S.; Clifford, J.; Klem, E.; Levina, L.; Sargent, E. H. *Nature* **2006**, *442*, 180−183.
(19) Hoogland, S.; Sukhovatkin, V.; Shukla, H.; Clifford, J.; Levina, L.; Sargent, E. H. *Opt. Express* **2008**, *16*, 6683−6691.
(20) Cavallini, A.; Polenta, L.; Rossi, M.; Stoica, T.; Calarco, R.; Meijers, R. J.; Luth, H. *Nano Lett.* **2007**, *7*, 2166−2170.
(21) Li, D.; Zhang, J.; Zhang, Q.; Xiong, Q. *Nano Lett.* **2012**, *12*, 2993−2999.
(22) Hanrath, T.; Korgel, B. A. *J. Am. Chem. Soc.* **2004**, *126*, 15466−15472.
(23) Ahn, Y. H.; Park, J. *Appl. Phys. Lett.* **2007**, *91*, 162102.
(24) Kim, C. J.; Lee, H. S.; Cho, Y. J.; Kang, K.; Jo, M. H. *Nano Lett.* **2010**, *10*, 2043−2048.
(25) Kim, C. J.; Lee, H. S.; Cho, Y. J.; Yang, J. E.; Lee, R. R.; Lee, J. K.; Jo, M. H. *Adv. Mater.* **2011**, *23*, 1025−1029.
(26) Fox, M. *Optical Properties of Solids*, Chapter 3; Oxford University Press: New York, 2001.
(27) Feng, N. N.; Feng, D.; Liao, S.; Wang, X.; Dong, P.; Liang, H.; Kung, C. C.; Qian, W.; Fong, J.; Shafiiha, R.; Luo, Y.; Cunningham, J.; Krishnamoorthy, A. V.; Asghari, M. *Opt. Express* **2011**, *19*, 7062−7067.
(28) Soref, R. A.; Bennett, B. R. *IEEE J. Quantum Electron.* **1987**, *QE-23*, 123−129.
(29) Pankove, J. I. *Optical Processes in Semiconductors*, Chapter 3; Dover: New York, 1971.
(30) Kingston, R. H. *J. Appl. Phys.* **1956**, *27*, 101−114.
(31) Hanrath, T.; Korgel, B. A. *J. Phys. Chem. B* **2005**, *109*, 5518−5524.
(32) Falk, A. L.; Koppens, F. H. L.; Yu, C. L.; Kang, K.; Snapp, N. D. L.; Akimov, A. V.; Jo, M. H.; Lukin, M. D.; Park, H. *Nat. Phys.* **2009**, *5*, 475−479.
(33) Frova, A.; Handler, P. *Phys. Rev.* **1965**, *137*, A1857−A1861.
(34) Schmid, M.; Oehme, M.; Kaschel, M.; Werner, J.; Kasper, E.; Schulze, J. *7th IEEE Int. Conf. Group IV Photonics* **2010**, 329−331.
(35) Van Van Eck, T. E.; Walpita, L. M.; Chang, W. S. C.; Wieder, H. H. *Appl. Phys. Lett.* **1986**, *48*, 451−453.
(36) Paige, E. G. S.; Rees, H. D. *Phys. Rev. Lett.* **1966**, *16*, 444−446.
(37) Moss, T. S. *J. Appl. Phys.* **1961**, *32*, 2136−2139.
(38) Jaeger, A.; Weiser, G. *Phys. Rev. B* **1998**, *58*, 10674−10682.